Analysis of Plasmonic Waveguides and Gratings Using Implicit Finite-Difference Methods

SHIBAYAMA, Jun / NAKANO, Hisamatsu / YAMAUCHI, Junji

(出版者 / Publisher)
Hindawi Publishing Corporation
(雑誌名 / Journal or Publication Title)
Advances in OptoElectronics / Advances in OptoElectronics
(開始ページ / Start Page)
1
(終了ページ / End Page)
6
(発行年 / Year)
2010-07-30

Hindawi Publishing Corporation
Advances in OptoElectronics
Volume 2011, Article ID 287284, 6 pages
doi:10.1155/2011/287284

Research Article

Analysis of Plasmonic Waveguides and Gratings Using Implicit Finite-Difference Methods

Jun Shibayama, Junji Yamauchi, and Hisamatsu Nakano

Faculty of Engineering, Hosei University, 3-7-2 Kajino-cho Koganei, Tokyo 184-8584, Japan

Correspondence should be addressed to Jun Shibayama, shiba@hosei.ac.jp

Received 12 June 2010; Accepted 30 July 2010

Academic Editor: Ana Vukovic

Various metal-insulator-metal- (MIM-) type plasmonic waveguides and gratings are investigated numerically. Three gratings are treated: one is formed by alternately stacking two kinds of MIM waveguides, another by periodic changes in the dielectric insulator materials of an MIM waveguide, and the other by a periodic variation of the air core width in an MIM waveguide. The dispersion property of each MIM waveguide of which the grating consists is analyzed using the implicit Yee-mesh-based beam-propagation method. It is shown that the third one has a relatively large effective index modulation of the guided mode with a simple grating structure, while maintaining a low propagation loss. Further examination is given to modifications of this grating structure. The transmission characteristics are examined using the frequency-dependent implicit locally one-dimensional FDTD method. We discuss how the modified grating structure affects the bandgap of the transmission characteristics.

1. Introduction

Recently, metal-insulator-metal- (MIM-) type plasmonic waveguides have received considerable attention, since compact optical circuits may be realized [1, 2]. The alternative effective index modulation of an MIM waveguide leads to a plasmonic waveguide Bragg grating that is one of the basic building blocks for small size plasmonic circuits. Three gratings have been mainly investigated: one is formed by alternately stacking two kinds of MIM waveguides (Figure 1(a)) [3], another by periodic changes in the dielectric insulator materials of an MIM waveguide (Figure 1(b)) [4], and the other by a periodic variation of the air core width in an MIM waveguide (Figure 1(c)) [5, 6]. We have numerically studied the sidelobe suppression of the latter one [7]. It is found that apodized and chirped gratings are quite effective in reducing the sidelobes. In addition, we have proposed a plasmonic microcavity offering a tunable resonance wavelength with varying an air core width. Note, however, that the characteristics of the above-mentioned three structures have not been compared in terms of an effective index modulation that is quite important to design gratings.

In this paper, we compare the basic characteristics of several MIM waveguides of which gratings are composed. The effective index versus core width of each MIM waveguide is calculated using the imaginary-distance Yee-mesh-based beam-propagation method (YM-BPM) [8]. It is shown that the grating with a periodic variation of the air core width (Figure 1(c)) yields a relatively large effective index modulation of the guided mode in the grating section, while maintaining a low propagation loss. We next examine the transmission coefficient of several gratings, that is, concave and convex gratings are calculated using the frequency-dependent locally one-dimensional finite-difference time-domain method (LOD-FDTD) [7, 9]. It is found that the convex grating gives a wide bandgap in the transmission coefficient because of a large index modulation. In addition, a slight modification to the plasmonic grating is found to yield a large variation in the bandgap, which is not easily obtainable using conventional dielectric gratings.

This paper is organized as follows. Section 2 gives the dispersion model of a metal and the brief explanations of the numerical techniques based on the efficient implicit schemes. Section 3 discusses the dispersion properties of each MIM waveguide with respect to the core width. Section 4 investigates the transmission coefficient of several modified gratings. Section 5 provides the concluding remarks.

2. Numerical Methods

2.1. Dispersion Model. The metal dispersion treated here is expressed by the following Drude model [5–7]:

$$\varepsilon_r(\omega) = \varepsilon_\infty + \frac{\omega_D^2}{j\omega(\nu_D + j\omega)}, \tag{1}$$

where ε_∞ is the dielectric constant of the material at infinite frequency, ω is the angular frequency, ω_D is the electron plasma frequency, and ν_D is the effective electron collision frequency.

2.2. Implicit Imaginary-Distance YM-BPM. The BPM is widely used to analyze optical waveguides. The BPM can also produce eigenmode fields quite efficiently, with the help of the imaginary-distance procedure. Note however that the conventional BPM cannot simultaneously offer all the electromagnetic fields, since it is based on the wave equation of either an electric or magnetic field. To simultaneously evaluate electric and magnetic field components, the YM-BPM has been developed on the basis of the explicit scheme [10]. The implicit scheme has also been introduced to the YM-BPM for efficient unconditionally stable calculations [8]. The use of Yee's mesh also means that the obtained eigenmode profile is readily used as an initial field in the following FDTD analysis. Detailed derivation of the three-dimensional YM-BPM can be found in [8], where the operator splitting is adopted in the propagation direction. Here, we present the resultant unsplit FD equations for the transverse magnetic (TM) waves suitable to the two-dimensional calculations as follows:

$$\begin{aligned}\left(b_+^2 - a_-^2\epsilon_{r,i+1/2} - \frac{b_+}{2}\delta_x^2\right)E_{x,i+1/2}^{l+1} &= \left(b_+b_- - a_+a_-\epsilon_{r,i+1/2} + \frac{b_+}{2}\delta_x^2\right)E_{x,i+1/2}^{l} \\ &\quad - (a_+b_+ - a_-b_-)H_{y,i+1/2}^{l},\end{aligned} \tag{2}$$

$$\begin{aligned}H_{y,i+1/2}^{l+1} = \frac{1}{a_-}\Bigg(a_+H_{y,i+1/2}^{l} + b_+E_{x,i+1/2}^{l+1} \\ -b_-E_{x,i+1/2}^{l} - \frac{1}{2}\delta_x^2E_{x,i+1/2}^{l+1} - \frac{1}{2}\delta_x^2E_{x,i+1/2}^{l}\Bigg),\end{aligned} \tag{3}$$

where

$$\begin{aligned}a_\pm &= jk_0\left(\frac{1}{\Delta z} \pm \frac{jk_0n_0}{2}\right), \\ b_\pm &= 4jk_0n_0 \pm \frac{k_0^2n_0^2}{2}, \\ \delta_x^2E_{x,i+1/2} &= \frac{c_1E_{x,i-1/2} - c_2E_{x,i+1/2} + c_3E_{x,i+3/2}}{\Delta x^2}\end{aligned} \tag{4}$$

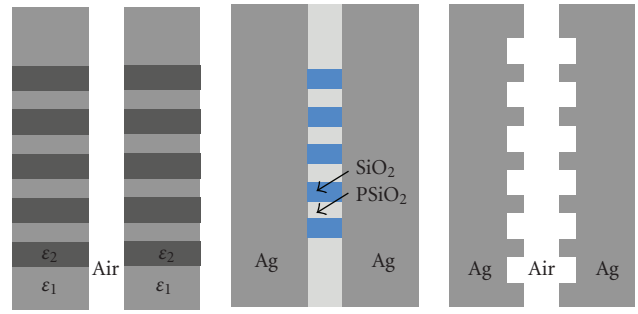

(a) grating 1 (b) grating 2 (c) grating 3

Figure 1: Configurations of plasmonic gratings. (a) grating 1: formed by alternately stacking two kinds of MIM waveguides, (b) grating 2: formed by periodic changes in the dielectric insulator materials of an MIM waveguide, and (c) grating 3: formed by a periodic variation of the air core width in an MIM waveguide.

in which

$$\begin{aligned}c_1 &= \frac{\epsilon_{r,i-1/2}}{\epsilon_{r,i}}, \\ c_2 &= \frac{\epsilon_{r,i+1/2}}{\epsilon_{r,i}} + \frac{\epsilon_{r,i+1/2}}{\epsilon_{r,i+1}}, \\ c_3 &= \frac{\epsilon_{r,i+3/2}}{\epsilon_{r,i+1}}.\end{aligned} \tag{5}$$

In the above equations, k_0, n_0, and ϵ_r, respectively, represent the free-space wavenumber, the reference refractive index, and the relative permittivity that is determined with (1) at a specific ω. As is observed, (2) gives a tridiagonal system of linear equations that are efficiently solved by the Thomas algorithm. Once E_x^{l+1} is obtained, H_y^{l+1} is explicitly calculated by (3).

To perform the eigenmode analysis, we apply the imaginary-distance procedure to the above YM-BPM [8], where the real propagation axis z is changed into the imaginary axis $j\tau$. This means that the phase variation of the propagating field turns into the amplification of the eigenmode field. The effective index gradually converges using the technique for renewing the reference refractive index n_0.

2.3. Frequency-Dependent Implicit LOD-FDTD Method. For the time-domain analysis of a metal in optical wavelengths, we have to utilize the frequency-dependent FDTD [11]. Note that the spatial sampling widths should be quite small for the analysis of a surface plasmon wave localized around the metal-dielectric interface. This gives rise to a small time step due to the Courant-Friedich-Levy (CFL) condition of the traditional explicit FDTD, resulting in long computational time. To efficiently perform the time-domain analysis, we have developed the frequency-dependent implicit LOD-FDTD [12, 13] that is free from the CFL condition [14]. In addition, to simply take into account the convolution integral, we have adopted the trapezoidal recursive convolution (TRC) technique requiring a single convolution [15, 16], which leads to almost the same accuracy as the piecewise

linear RC (PLRC) counterpart requiring two convolution integrals [17]. We here present the basic equation (TM waves) of the frequency-dependent LOD-FDTD based on the TRC technique for the Drude model as follows [7, 9]:

$$E_x' = E_x^n, \tag{6a}$$

$$E_z' = \frac{\varepsilon_\infty - \chi_D^0/2}{\varepsilon_\infty + \chi_D^0/2} E_z^n + \frac{1}{\varepsilon_\infty + \chi_D^0/2}\phi_z^n + \frac{c\Delta t}{2\left(\varepsilon_\infty + \chi_D^0/2\right)}\left(\frac{\partial H_y'}{\partial x} + \frac{\partial H_y^n}{\partial x}\right), \tag{6b}$$

$$\frac{H_y' - H_y^n}{\Delta t/2} = c\left(\frac{\partial E_z'}{\partial x} + \frac{\partial E_z^n}{\partial x}\right), \tag{6c}$$

for the first step and

$$E_z^{n+1} = E_z', \tag{7a}$$

$$E_x^{n+1} = \frac{\varepsilon_\infty - \chi_D^0/2}{\varepsilon_\infty + \chi_D^0/2} E_x' + \frac{1}{\varepsilon_\infty + \chi_D^0/2}\phi_x^n - \frac{c\Delta t}{2\left(\varepsilon_\infty + \chi_D^0/2\right)}\left(\frac{\partial H_y^{n+1}}{\partial z} + \frac{\partial H_y'}{\partial z}\right), \tag{7b}$$

$$\frac{H_y^{n+1} - H_y'}{\Delta t/2} = -c\left(\frac{\partial E_x^{n+1}}{\partial z} + \frac{\partial E_x'}{\partial z}\right), \tag{7c}$$

for the second step, where E' and H' represent the intermediate fields, and c is the speed of light in a vacuum. The parameters used above are expressed as follows:

$$\phi_\delta^n = \frac{E_\delta^n + E_\delta^{n-1}}{2}\Delta\chi_D^0 + e^{-\nu_D\Delta t}\phi_\delta^{n-1},$$

$$\chi_D^0 = \frac{\omega_D^2}{\nu_D}\left\{\Delta t - \frac{1}{\nu_D}\left(1 - e^{-\nu_D\Delta t}\right)\right\}, \tag{8}$$

$$\Delta\chi_D^0 = -\frac{\omega_D^2}{\nu_D^2}\left(1 - e^{-\nu_D\Delta t}\right)^2$$

in which $\delta = x$ or z. Note that the normalized expression of field components is used. The equations for the TRC-LOD-FDTD are simpler than those for the PLRC-LOD-FDTD [13]. In the first step, we substitute (6c) into (6b) and implicitly solve the resultant equation using the Thomas algorithm. Then, (6c) is explicitly solved. In the second step, the equations are calculated in the same way as in the first step. It should be noted that the frequency-dependent implementation of the LOD-FDTD is much simpler than that of the frequency-dependent alternating-direction implicit (ADI) FDTD.

3. Dispersion Properties of MIM Waveguides

It is important to calculate the effective indexes of waveguides of which the grating is composed, since the alternative effective index modulation predominates grating characteristics. Therefore, we first calculate the dispersion property of various MIM waveguides with respect to the core width. To obtain the effective index, we use the YM-BPM with the imaginary-distance procedure.

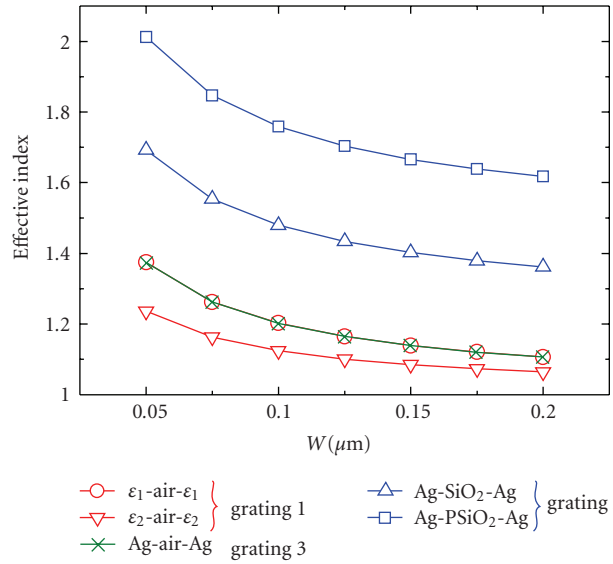

Figure 2: Effective index of the MIM waveguide.

Three plasmonic gratings treated here are as follows (see Figure 1): one is formed by alternately stacking two kinds of MIM waveguides (grating 1) [3], another by periodic changes in the dielectric insulator materials of an MIM waveguide (grating 2) [4], and the other by a periodic variation of the dielectric insulator width in an MIM waveguide (grating 3) [5, 6]. For grating 1, $\omega_D = 15$ eV and $\nu_D = 0.01$ eV are used for ϵ_1, and $\omega_D = 9$ eV and $\nu_D = 0.001$ eV are for ϵ_2, where $\epsilon_\infty = 1$ is commonly adopted (metals are not specified) [3]. For grating 2, the permittivity of Ag is determined with $\epsilon_\infty = 3.7$, $\omega_D = 9.1$ eV, and $\nu_D = 0.018$ eV (in consistent with the experimental results), and those of SiO_2 and $PSiO_2$ are 1.46^2 and 1.23^2, respectively [4]. For grating 3, the Ag permittivity is the same as that used for grating 2.

Figure 2 shows the effective index of the MIM waveguide of which each grating is composed, as a function of core width W at a wavelength of $\lambda = 1.55\,\mu$m. In Figure 2, the results of ϵ_1-air-ϵ_1 and ϵ_2-air-ϵ_2 are presented for grating 1, those of Ag-SiO_2-Ag and Ag-$PSiO_2$-Ag are for grating 2, and the result of Ag-air-Ag is for grating 3. It is interesting to note that the effective index becomes large as the core width W is decreased. This contrasts to the case of a conventional dielectric waveguide, where the effective index becomes small as the core width is decreased.

Now, we pay attention to the effective index difference Δn_e, when the two MIM waveguides are used to form gratings. For grating 1, Δn_e is calculated to be 0.138 at $W = 0.05\,\mu$m and 0.078 at $W = 0.1\,\mu$m from the results in Figure 2. For grating 2, Δn_e is to be 0.329 at $W = 0.05\,\mu$m and 0.278 at $W = 0.1\,\mu$m. For grating 3, Δn_e is evaluated

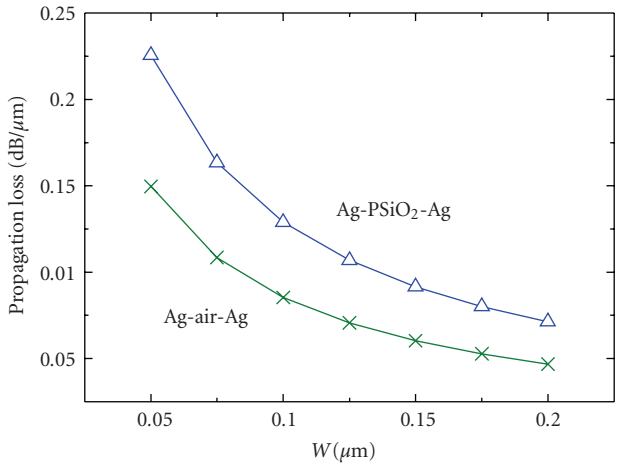

Figure 3: Propagation loss.

to be 0.172 with a combination of $W_1 = 0.05\,\mu$m and $W_2 = 0.1\,\mu$m. As a result, a large Δn_e can be obtained for grating 2, although three materials (Ag, SiO_2, and $PSiO_2$) are required. In contrast, for grating 3, a relatively large Δn_e is obtainable with a simple grating structure (Ag-air-Ag). The propagation losses for the latter two cases are calculated in Figure 3. It is seen that the propagation loss for Ag-air-Ag is smaller than that for Ag-$PSiO_2$-Ag. Therefore, we choose the Ag-air-Ag waveguide (grating 3) because of a relatively large Δn_e and a low propagation loss, and investigate various modified gratings in the following analysis.

4. Characteristics of Modified Plasmonic Gratings

Using the frequency-dependent LOD-FDTD, we investigate four plasmonic gratings consisting of the Ag-air-Ag MIM waveguide with the input core width W_1 being fixed. The reference grating (concave type) is shown in Figure 4(a), the parameters of which are $W_1 = 0.1\,\mu$m, $W_2 = 0.15\,\mu$m, $L_p = 0.660\,\mu$m, and $L_s = 0.292\,\mu$m. The number of the grating period is 14. The normalized transmission coefficient for concave type is presented in Figure 5(a), which is indicated by the black solid line. Note that the Bragg condition is expressed by $k[n_{e1}(L_p - L_s) + n_{e2}L_s] = (2m + 1)\pi$. For this grating, the effective indexes are found to be $n_{e1} = 1.20204$ and $n_{e2} = 1.139$ in Figure 2. Then, the Bragg wavelength is calculated to be $\simeq 1.55\,\mu$m from the above condition, which almost agrees with the center wavelength of the transmission coefficient for concave type.

Next, we examine another grating with $W_3 = 0.05\,\mu$m shown in Figure 4(b) (convex type). For this grating, the effective index for W_3 is $n_{e3} = 1.37428$, leading to a Bragg wavelength of $\simeq 1.69\,\mu$m (recall that the effective index for the MIM waveguide becomes large, as the core width is reduced). The red solid line in Figure 5(a) represents the coefficient for convex type, in which the bandgap is found to be much wider than that for concave type. This is due to the fact that the bandgap becomes wide as the contrast between the effective

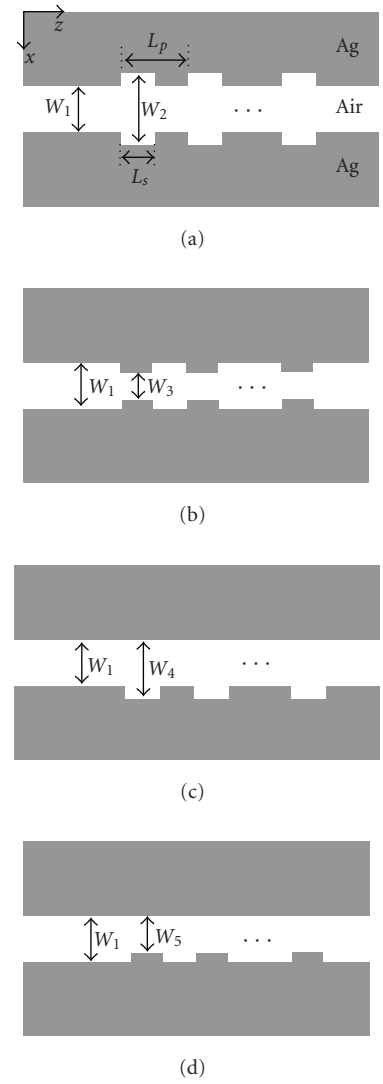

Figure 4: Various plasmonic gratings. (a) concave type, (b) convex type, (c) flat-concave type, and (d) flat-convex type.

indexes of alternating layers is increased [4]. In this case, the index contrast for convex type is 0.172, while that for concave type is 0.063, leading to the wide bandgap for convex type. As a result, the convex type plasmonic grating can yield a wide bandgap, compared with the concave type where a large effective index modulation cannot be obtained for a large W as shown in Figure 2.

We further modify the gratings, in which the one side of the metals for concave type is replaced with a flat metal, as shown in Figure 4(c) (flat-concave type). For this type, the effective index of the $W_4 (= 0.125\,\mu$m) section is 1.165, resulting in a Bragg wavelength of $\simeq 1.56$. This Bragg wavelength is close to that without the modification ($\simeq 1.55$ for concave type). It is therefore expected that the bandgap of the transmission coefficient for flat-concave type is reduced with the Bragg wavelength being almost fixed. The black dotted line in Figure 5(b) is the coefficient for flat-concave type. As expected, the bandgap becomes narrower than that

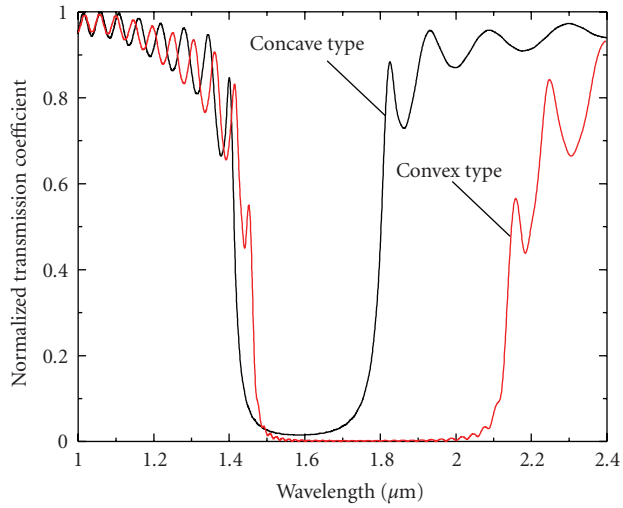

(a) Comparison between concave type (Figure 4(a)) and convex type (Figure 4(b))

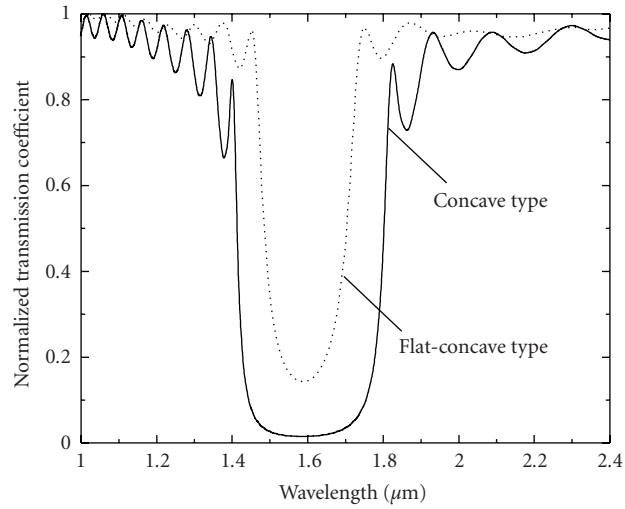

(b) Comparison between concave type (Figure 4(a)) and flat-concave type (Figure 4(c))

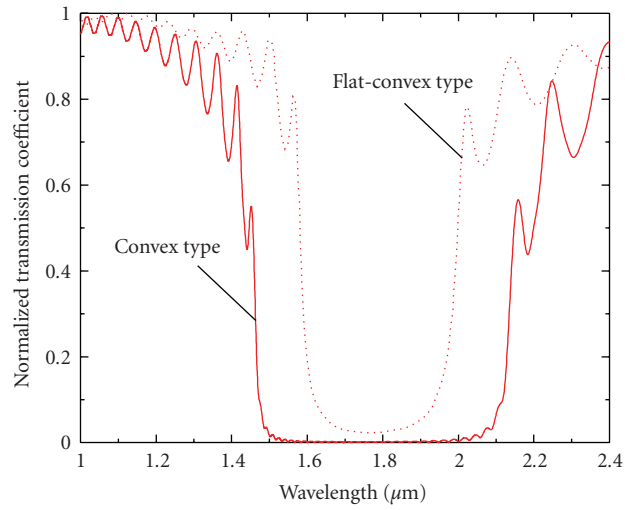

(c) Comparison between convex type (Figure 4(b)) and flat-convex type (Figure 4(d))

FIGURE 5: Normalized transmission coefficient.

for concave type, while maintaining the Bragg wavelength. This is almost true for flat-convex type (the one side of the metals for convex type is taken flat as shown in Figure 4(d)), in which the coefficient is approximately centered in that for convex type (see Figure 5(c)). It should be noted that even the slight modification to the plasmonic grating structure shown above leads to a large variation in the bandgap, which is not easily obtainable from conventional dielectric gratings.

Finally, we point out the efficiency of the LOD-FDTD. In the above analysis, we have used a time step of 0.102 fs ten times as large as that determined from the CFL condition of the explicit FDTD. As a result, the computational time of the LOD-FDTD is successfully reduced to 30% of the explicit counterpart, where a PC with Core2Quad processor (2.66 GHz) is used. The LOD-FDTD is suitable for the analysis of plasmonic devices in which quite small sampling widths should be required.

5. Conclusion

We have investigated the dispersion characteristics of several MIM waveguides and examined the transmission coefficient of several modified gratings. First, we briefly present the numerical techniques, that is, the implicit YM-BPM for the eigenmode analysis and the frequency-dependent LOD-FDTD for the time-domain analysis. Next, we calculate the effective index of each MIM waveguide. A simple MIM waveguide made of Ag-air-Ag is found to provide a relatively large effective index modulation, maintaining a low propagation loss. We further calculate the characteristics of concave and convex gratings. The convex grating is shown to yield a wide bandgap of the transmission coefficient. Finally, we modify the grating structures to study the effect on the transmission coefficient. A slight modification to the grating leads to a significant change in the transmission coefficient. Applications to three-dimensional gratings are now under consideration.

Acknowledgments

The authors would like to thank Mr. Ryo Takahashi for calculating the characteristics of plasmonic waveguides and gratings. This work was supported in part by MEXT, Grant-in-Aid for Young Scientists (B) (21760266).

References

[1] K. Tanaka and M. Tanaka, "Simulations of nanometric optical circuits based on surface plasmon polariton gap waveguide," *Applied Physics Letters*, vol. 82, no. 8, pp. 1158–1160, 2003.

[2] J. Takahara and F. Kusunoki, "Guiding and nanofocusing of two-dimensional optical beam for nanooptical integrated circuits," *IEICE Transactions on Electronics*, vol. E90-C, no. 1, pp. 87–94, 2007.

[3] B. Wang and G. P. Wang, "Plasmon Bragg reflectors and nanocavities on flat metallic surfaces," *Applied Physics Letters*, vol. 87, no. 1, Article ID 013107, 3 pages, 2005.

[4] A. Hosseini and Y. Massoud, "A low-loss metal-insulator-metal plasmonic bragg reflector," *Optics Express*, vol. 14, no. 23, pp. 11318–11323, 2006.

[5] Z. Han, E. Forsberg, and S. He, "Surface plasmon Bragg gratings formed in metal-insulatormetalwaveguides," *IEEE Photonics Technology Letters*, vol. 19, no. 2, pp. 91–93, 2007.

[6] L. Yuan and Y. Y. Lu, "A recursive-doubling Dirichlet-to-Neumann-map method for periodic waveguides," *Journal of Lightwave Technology*, vol. 25, no. 11, pp. 3649–3656, 2007.

[7] J. Shibayama, A. Nomura, R. Ando, J. Yamauchi, and H. Nakano, "A frequency-dependent LOD-FDTD method and its application to the analyses of plasmonic waveguide devices," *IEEE Journal of Quantum Electronics*, vol. 46, no. 1, pp. 40–49, 2010.

[8] J. Yamauchi, T. Mugita, and H. Nakano, "Implicit Yee-mesh-based finite-difference full-vectorial beam-propagation method," *Journal of Lightwave Technology*, vol. 23, no. 5, pp. 1947–1955, 2005.

[9] J. Shibayama, R. Ando, A. Nomura, J. Yamauchi, and H. Nakano, "Simple trapezoidal recursive convolution technique for the frequency-dependent FDTD analysis of a drude-lorentz model," *IEEE Photonics Technology Letters*, vol. 21, no. 2, pp. 100–102, 2009.

[10] S. M. Lee, "Finite-difference vectorial-beam-propagation method using Yee's discretization scheme for modal fields," *Journal of the Optical Society of America A*, vol. 13, no. 7, pp. 1369–1377, 1996.

[11] A. Taflove and S. C. Hagness, *Computational Electrodynamics: The Finite-Difference Time-Domain Method*, Artech House, Norwood, Mass, USA, 3rd edition, 2005.

[12] J. Shibayama, R. Takahashi, J. Yamauchi, and H. Nakano, "Frequency-dependent LOD-FDTD implementations for dispersive media," *Electronics Letters*, vol. 42, no. 19, pp. 1084–1086, 2006.

[13] J. Shibayama, R. Takahashi, J. Yamauchi, and H. Nakano, "Frequency-dependent locally one-dimensional FDTD implementation with a combined dispersion model for the analysis of surface plasmon waveguides," *IEEE Photonics Technology Letters*, vol. 20, no. 10, pp. 824–826, 2008.

[14] J. Shibayama, M. Muraki, J. Yamauchi, and H. Nakano, "Efficient implicit FDTD algorithm based on locally one-dimensional scheme," *Electronics Letters*, vol. 41, no. 19, pp. 1046–1047, 2005.

[15] R. Siushansian and J. LoVetri, "Comparison of numerical techniques for modeling electromagnetic dispersive media," *IEEE Microwave and Guided Wave Letters*, vol. 5, no. 12, pp. 426–428, 1995.

[16] R. Siushansian and J. LoVetri, "Efficient evaluation of convolution integrals arising in FDTD formulations of electromagnetic dispersive media," *Journal of Electromagnetic Waves and Applications*, vol. 11, no. 1, pp. 101–117, 1997.

[17] D. F. Kelley and R. I. Luebbers, "Piecewise linear recursive convolution for dispersive media using FDTD," *IEEE Transactions on Antennas and Propagation*, vol. 44, no. 6, pp. 792–797, 1996.